remote sensing

MDPI

Article

Physiographic Controls on Landfast Ice Variability from 20 Years of Maximum Extents across the Northwest Canadian Arctic

Eleanor E. Wratten [1,*], Sarah W. Cooley [2], Paul J. Mann [1], Dustin Whalen [3], Paul Fraser [3] and Michael Lim [1]

[1] Faculty of Engineering and Environment, Northumbria University, Newcastle upon Tyne NE1 8ST, UK; eleanor.e.wratten@northumbria.ac.uk (E.E.W.); paul.mann@northumbria.ac.uk (P.J.M.); michael.lim@northumbria.ac.uk (M.L.)
[2] Department of Geography, University of Oregon, Eugene, OR 97403, USA; scooley2@uoregon.edu
[3] Geological Survey of Canada (Atlantic), Natural Resources Canada, Dartmouth, NS B3B, Canada; dustin.whalen@nrcan-rncan.gc.ca (D.W.); paul.fraser@nrcan-rncan.gc.ca (P.F.)
* Correspondence: eleanor.e.wratten@northumbria.ac.uk

Abstract: Landfast ice is a defining feature among Arctic coasts, providing a critical transport route for communities and exerting control over the exposure of Arctic coasts to marine erosion processes. Despite its significance, there remains a paucity of data on the spatial variability of landfast ice and limited understanding of the environmental processes' controls since the beginning of the 21st century. We present a new high spatiotemporal record (2000–2019) across the Northwest Canadian Arctic, using MODIS Terra satellite imagery to determine maximum landfast ice extent (MLIE) at the start of each melt season. Average MLIE across the Northwest Canadian Arctic declined by 73% in a direct comparison between the first and last year of the study period, but this was highly variable across regional to community scales, ranging from 14% around North Banks Island to 81% in the Amundsen Gulf. The variability was largely a reflection of 5–8-year cycles between landfast ice rich and poor periods with no discernible trend in MLIE. Interannual variability over the 20-year record of MLIE extent was more constrained across open, relatively uniform, and shallower sloping coastlines such as West Banks Island, in contrast with a more varied pattern across the numerous bays, headlands, and straits enclosed within the deep Amundsen Gulf. Static physiographic controls (namely, topography and bathymetry) were found to influence MLIE change across regional sites, but no association was found with dynamic environmental controls (storm duration, mean air temperature, and freezing and thawing degree day occurrence). For example, despite an exponential increase in storm duration from 2014 to 2019 (from 30 h to 140 h or a 350% increase) across the Mackenzie Delta, MLIE extents remained relatively consistent. Mean air temperatures and freezing and thawing degree day occurrences (over 1, 3, and 12-month periods) also reflected progressive northwards warming influences over the last two decades, but none showed a statistically significant relationship with MLIE interannual variability. These results indicate inferences of landfast ice variations commonly taken from wider sea ice trends may misrepresent more complex and variable sensitivity to process controls. The influences of different physiographic coastal settings need to be considered at process level scales to adequately account for community impacts and decision making or coastal erosion exposure.

Keywords: arctic; MODIS; landfast ice extent; scale; topographic setting; storms; environmental processes; community; coastal erosion

Citation: Wratten, E.E.; Cooley, S.W.; Mann, P.J.; Whalen, D.; Fraser, P.; Lim, M. Physiographic Controls on Landfast Ice Variability from 20 Years of Maximum Extents across the Northwest Canadian Arctic. *Remote Sens.* **2022**, *14*, 2175. https://doi.org/10.3390/rs14092175

Academic Editors: Juha Karvonen and Anton Korosov

Received: 14 February 2022
Accepted: 25 April 2022
Published: 30 April 2022

Publisher's Note: MDPI stays neutral with regard to jurisdictional claims in published maps and institutional affiliations.

1. Introduction

It is common for studies to generalize the term 'sea ice', often not differentiating between pack ice, drifting ice, and specifically landfast ice. Landfast ice is a critical

component of the Arctic coast and accounts for ≈13% of the Northern Hemisphere's areal sea ice cover, with ≈30% of all landfast ice occurring throughout the Canadian Arctic [1,2]. Landfast ice is attached to or near the coastline, extending perpendicular to the coastline without becoming grounded or drifting [3,4]. It forms a rigid boundary which occupies the meeting between atmospheric, marine, and terrestrial environments [5–7]. Across the Northwest Canadian Arctic, landfast ice forms between October and November, stabilizing soon after and reaching maximum extent in early May, before rapidly breaking up [5,8,9]. Specifically, formation occurs when temperatures remain consistently below 0 °C and thawing commences when solar radiation increases, showing interseasonal and interannual variability [4,5,10,11]. Previous research has suggested landfast ice decline may 'outpace' the current pan-Arctic Sea ice decline signal [12,13]. Therefore, landfast ice should be considered as a specific and distinct component when addressing the impacts of climatic changes on the nearshore zone of Arctic coasts.

Maximum landfast ice extent (MLIE) changes have varied more than landfast ice thickness across the Northwest Passage since the beginning of the 21st century [1]. The influence of physiographic controls on MLIE have been limited by a lack of spatial and temporal observational data at a sufficiently resolved scale. Physiographic controls, in this context, can be defined by the various controls on landfast ice from static settings such as topography or bathymetry, contrasted against dynamic environmental drivers such as temperature or storminess. Static controls, including topographic setting and bathymetry, play an important role in understanding landfast ice behavior [14–16]. Regarding topographic setting, restrictive geometry, such as islands, have been shown to impact landfast ice presence [14]. Bathymetric controls have also previously been identified, with the 30 m isobath shown to influence landfast ice extents [5,17,18], especially when these shallow waters have the necessary amount of grounded ice ridges to anchor and stabilize landfast ice [16,19,20]. However, there is a notable lack of studies that directly focus on how contrasting topographic settings can affect landfast ice extents, even across the same regional coastline. Whilst static environmental controls affect the spatial distribution of landfast ice, they do not impact the temporal interannual variation in MLIE, unlike dynamic controls [8,21,22]. The majority of dynamic controls on landfast ice variability, such as storm duration, mean air temperature (MAT), and freezing and thawing degree day occurrence (FDD and TDD), are directly related to climatic changes and influence economic, ecological, social, and environmental impacts across the Northwest Canadian Arctic [10,23–27].

The Arctic has undergone transformative climate change, with profound implications for oil and natural gas extraction industries and transportation, with ice roads becoming increasingly vulnerable over the past few decades [28,29]. These industries depend on stable sea ice with little interannual variability to plan valuable shipping and travel routes [9,10]. Negative ecological impacts, such as increased marine mammal injuries from more marine traffic, have also been associated with longer open water seasons. Polynya are areas of open water that form between MLIE edges and drifting sea ice and create hotspots for high ecological productivity [30]. Therefore, declining landfast ice extents will reduce the surface area of MLIE edges, hence reducing ecological diversity. Ecologists require better annual resolution landfast ice data to understand the current and future impacts on species habitats [25]. The seaward MLIE edge provides a crucial habitat for macrofauna such as polar bears and ringed seals, which are crucial for coastal community stability due to their strong socioeconomic and cultural dependence on landfast ice [31]. Canadian Arctic coastal communities have resided and utilized these coastlines for ≈10,000 years for seasonal hunting, fishing, and trapping [32,33] and they have witnessed a reduction in ringed seal pups born, as a result of less stable and reduced landfast ice habitats in recent decades [34,35]. Since the beginning of the century, the time and finances required to hunt and fish in the traditional manner have increased due to inconsistent MLIE patterns; however, local communities still depend on this as a source of food and income, with more than 75% of meat and fish coming from subsistence hunting and fishing [36,37]. Furthermore, the lack of sufficient data on landfast ice interannual variability

and decline means local people rely on more readily obtained regional sea ice signals. The local inaccuracy of these regional datasets reduces hunting success and threatens the safety of these coastal communities, leading to accidents and fatalities [38]. Regarding marine erosion, with consistently lower MLIE and earlier breakup, vulnerability is increased due to more days per year of direct wave to cliff contact, alongside increasing storm intensity and duration [5,39,40]. Arctic marine erosion is further exacerbated by coastal permafrost thaw, subsidence, and collapse, which provide positive feedbacks linked to declining landfast ice barrier protection and can accelerate the release of carbon and methane, negatively contributing to further global warming [41–45].

Most of the early satellite mapping conducted in the Northwest Canadian Arctic were ice maps produced by services, such as the 'Canadian Ice Survey'. Although they provide high quality spatial ice information, often the resolutions are not sufficiently resolved to identify and analyze landfast ice at process levels surrounding local coastal communities and can be considerably affected by cloud cover [18,46]. Thus in recent years, various ice mapping approaches have used MODIS satellite imagery due to its large spatial and temporal scale availability [15,25,47–50]. MODIS satellite imagery is utilized in this study as it suits landfast ice mapping in the complex topography of the Northwest Canadian Arctic due to its unique high temporal resolution and free open access data source availability [9,51,52].

This study aims to provide new landfast ice observational data, particularly MLIE, at sufficient temporal and spatial resolution to identify and analyze key static and dynamic controls on ice variability across the Northwest Canadian Arctic. These new datasets establish the necessary metrics and appropriate scales to accurately monitor landfast ice changes in the future. We first describe our study area, data availability, and methodological approach. Next, we provide an overview of the spatial and temporal patterns of MLIE for the previous 20 years, including analysis of potential correlations with static and dynamic controls. Finally, we conclude with a discussion on the importance of differentiating between landfast ice and sea ice, the community reliance on and vulnerability to landfast ice variability, and the appropriate metrics and scales for landfast ice specific research.

2. Materials and Methods

2.1. Study Area

The Northwest Canadian Arctic coastline represents a varied complex topographic setting (68°N–78°N and 115°W–145°W; Figure 1). The low-lying deltaic coasts at the mouth of the Mackenzie contrast with steep cliffs and slumps of the outer islands, whereas the topographic setting of the Amundsen Gulf consists of complex bays, channels, and straits. This topographic variety is less evident in the relatively uniform steep cliffs of both West and North Banks Island. The Northwest Canadian Arctic is a critical area of the Arctic where landfast ice extents remain poorly understood but influence both vital shipping routes and many coastal communities. Understanding the detailed patterns and controls on landfast ice extent in the Northwest Canadian Arctic enables an essential new level of detail, highlighting four regional sections: the Mackenzie Delta, the Amundsen Gulf, West Banks Island, and North Banks Island. These regions were chosen to account for a distinction in topographic setting, bathymetry, temperature, windspeed, and direction, allowing both static and dynamic controls on ice variability and its wider implications to be explored.

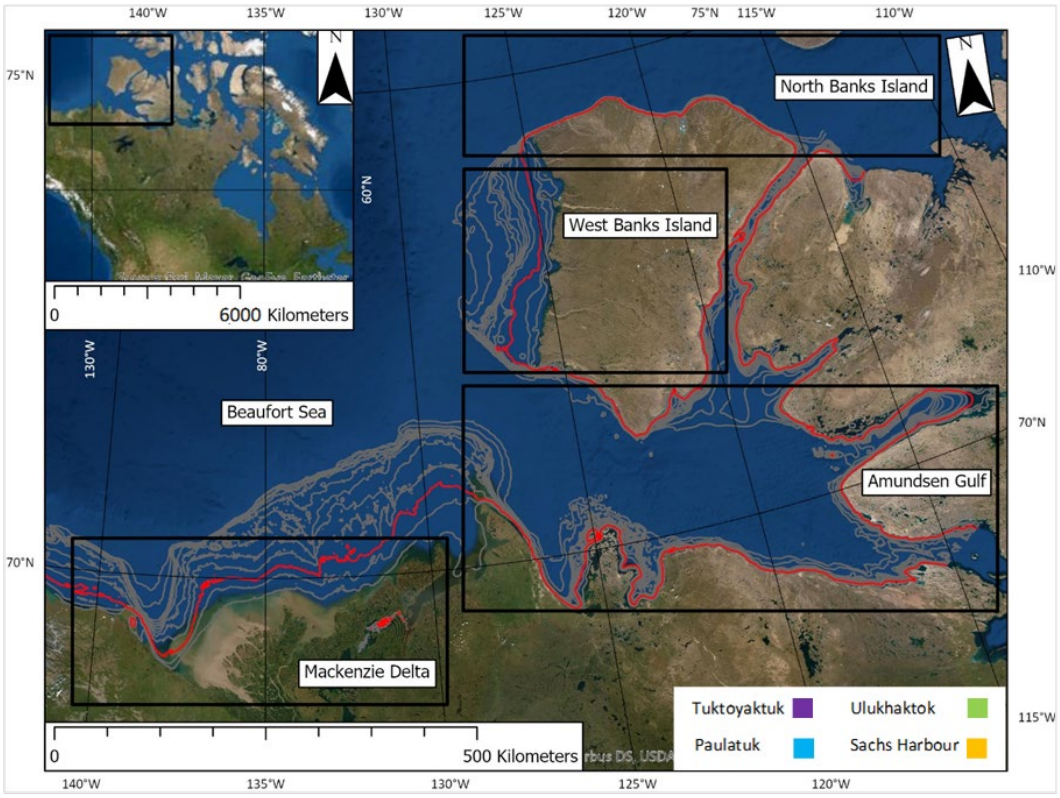

Figure 1. This Northwest Canadian Arctic study area covers ≈3200 km of permafrost coastlines. Four regions have been identified for the purpose of this study: Mackenzie Delta (≈482 km), Amundsen Gulf (≈1854 km), West Banks Island (≈275 km), and North Banks Island (≈216 km). Example communities with nearby weather stations used for analysis of dynamic controls are shown with coloured boxes: Tuktoyaktuk (purple), Paulatuk (blue), Ulukhaktok (green), and Sachs Harbour (yellow). The red line indicates the 30 m isobath and shows its spatial variability across the study area, the brown lines represent the bathymetric range from 10 m to 30 m; these were extracted using the GEBCO_2021 Grid [53].

2.2. Data Availability and Preprocessing

Landfast ice has been mapped using an atmospherically corrected MODIS Level 2 product, also referred to as MOD09GQ, maintained by NASA EOSDIS LP DAAC at the USGS Center. MODIS-Terra started capturing images on the 24 February 2000 after being launched by NASA on the 18 December 1999 [25]. The satellite is still capturing images today and thus is used here to map MLIE due to its high collection frequency allowing a detailed 20-year monitoring record to be produced, as global coverage is achieved every 1–2 days (and even higher revisit times in the Arctic). The MODIS satellite has a 2330 km view swath with 36 spectral bands ranging from visible to thermal infrared (0.45 µm to 14.4 µm) with a resolution of 250 m. It is on a 16 day repeat cycle and has a sun-synchronous orbit with a descending node at 10:30 UTC. The high spatiotemporal resolution enables the distinction of landfast ice patterns across this expansive region of Arctic, covering ≈3200 km of coastline. Clouds and shadows were masked by the MOD09GA product, then resampled to 250 m pixel resolution to match the original MOD09GQ product set using the approach outlined in previous work [9,51]. For static controls, the bathymetric data were generated using GEBCO_21 Grid [53]. Weather data pertaining to storm frequency, duration, and mean air temperature from the Environment and Climate Change Canada (ECCC) were available from the stations proximal to the MLIE position tested in each region; these were Tuktoyaktuk, Cape Parry, Sachs Harbour, and Mould Bay from 2000 to 2019 (https://weather.gc.ca/ (accessed on 12 May 2021)) using the R package *weathercan* (https://github.com/ropensci/weathercan/ (accessed on 12 May 2021)).

2.3. MLIE Mapping

While sea ice is generally easy to distinguish in MODIS imagery, identifying the position of landfast ice edges can be challenging due to the frequent presence of cloud cover and/or other image artifacts. To facilitate easier detection of the ice edge position, 30-day ice occurrence composites were made from Band 2 (841–876 nm) MOD09GQ imagery. First, clouds and land were masked out of each image using the MOD09GA cloud mask as described above and with a high resolution coastline shapefile (available at: https://open.canada.ca/data/en/dataset/a883eb14-0c0e-45c4-b8c4-b54c4a819edb (8 November 2020)). Next, ice versus water was classified by applying a simple threshold (water = reflectance < 0.1; reflectance is the MOD09GQ digital number multiplied by 0.001) following the methods described in [9]. These ice versus water classified images were then combined to produce an ice occurrence image defined as:

$$Ice\ Occurrence = \frac{\sum_{d-30}^{d} ice\ \ observation}{\sum_{d-30}^{d} cloud-free\ observation} \quad (1)$$

Here d is the day of year, *ice observation* refers to whether a pixel was classified as ice, and *cloud–free observation* refers to whether a pixel was classified as cloud-free (for example, was not masked out by the cloud mask). Note *ice occurrence* is calculated on a per pixel scale. Given that a key defining feature of landfast ice is the formation of a polynya at the landfast ice edge [30], the occurrence maps clearly highlight the ice edge position and remove any artifacts due to cloud cover or poor quality imagery (Figure 2B).

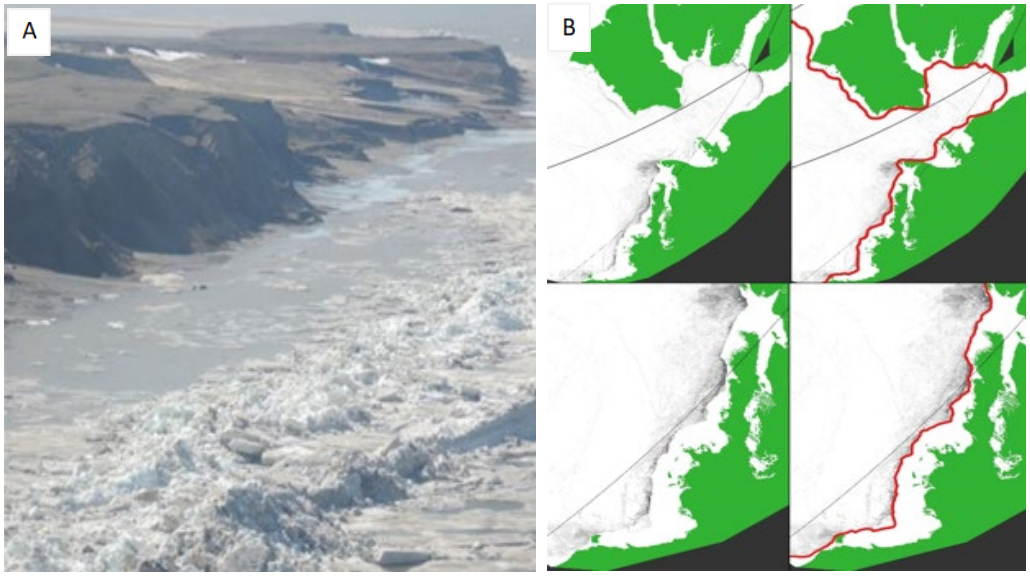

Figure 2. (**A**) Landfast ice during spring break-up along Hooper Island in 2016 along the Beaufort Sea coastline, acting as a barrier to marine erosion. (**B**) Ice occurrence images with the manually delineated landfast ice edge overlaid. Landfast ice edge extents can be seen as dark grey lines in the left-hand side panels relative to the land mask in green. Red lines on the right panels show digitized MLIE.

Ice occurrence images calculated from the 4th of May each year were analyzed to define a consistent temporal point to determine the MLIE. This date was chosen as it is prior to the onset of rapid spring breakup [9], allowing clear, distinguishable MLIE edges. Interannual extents were digitized using a stylus. The 2010 imagery did not sufficiently resolve the MLIE as the ice edge was too narrow and unstable to be accurately resolved in MODIS imagery, particularly in the narrow straits southeast of the Amundsen Gulf. Therefore, data from 2010 have been excluded from further analysis. The digitization

produced shapefile layers that were subsequently analyzed in a GIS environment to map patterns and quantify annual variations. The reliability of the approach was assessed by repeating the digitization three times over the entire study area, which instilled confidence in the chosen method and results. Once the MLIE lines for each year (2000–2019) were plotted, the average MLIE distance from the coastline was calculated for the study area and each of the four regions individually to enable the assessment of spatial and temporal variations and their relation to static and dynamic controls. Comparing these controls against the study area average, regional average, and a consistently chosen point in each region allowed a range of scales to be identified.

2.4. Analysis of Dynamic Controls on MLIE

In the absence of sufficient wave data, windspeed and duration are used to categorize storms [54–56]. Specifically, to analyze the impact of storminess on MLIE change across each region for every year, the windspeed data were extracted from the closest weather station with the highest quality temporal hourly data. Then, windspeeds ≥38 km/h and lasting ≥6 h with few lulls and shoulders (<2 h of windspeed <38 km/h in a storm) were identified as in previous studies [54–56]. Further analysis compared the impact of all storms with only those storms with wind direction facing the MLIE edge to explore if the directional impact of storm factors (windblown waves) had greater explanatory influence on MLIE pattern variability. The directions of windspeed were filtered as follows: Mackenzie Delta (290°–20°, WNW–NNE), Amundsen Gulf (250°–340°, NW–WNW), West Banks Island (235°–325°, W–NW), and North Banks Island (235°–325°, W–NW). Storm duration was chosen rather than storm count to account for the exposure of landfast ice to storm conditions, as a count may not adequately describe particularly long storms. Mean air temperature (MAT) was calculated by averaging hourly temperature data. This allowed both FDD (<0 °C) and TDD (>0 °C) to be analyzed by filtering air temperature and creating a count. Each dynamic control was tested for the previous 1, 3, and 12-month periods preceding May 4th per year distinguished as the MLIE in this study.

3. Results

3.1. Spatial and Temporal Pattern Variability of Maximum Landfast Ice Extent

Average MLIE distances calculated across the entire study area coastline (Figure 3) declined by 73% in a direct comparison between the individual years of 2000 and 2019. However, MLIE positions were highly dynamic and variable, progressing through both landfast ice rich and poor periods. Across the study area average, the 5–8-year cycling from low to high and back to low landfast ice extents show no discernible trend in MLIE over time. This contrasts with relatively continuous decline of sea ice extent noted elsewhere, which comprises of and does not distinguish between pack ice, drifting ice, and landfast ice [57–59]. Although multiyear MLIE cycling was observed across the entire study area, the magnitudes varied between regions. More pronounced cycles were recorded in the Amundsen Gulf region and less pronounced but still visible cycles in all other regions (Figure 3). There were similarities in the timing of rich and poor periods across regions. For example, from 2018 to 2019 all regions lie within a −31% and −44% average MLIE decline. However, there were also years where contrasts in MLIE patterns between regions were seen such as during 2001–2002, when all regions apart from North Banks Island switched from a severe poor MLIE period to a richer one. Specifically, both Amundsen Gulf and West Banks Island record large changes to a richer period by 360% and 187% in 2002, when in the previous year declines of −80% and −68% were recorded. The severity of interannual fluctuations can be clearly seen from the Amundsen Gulf region, as 7 out of the 19 years recorded have over 50% change in MLIE from one year to the next (Table 1).

In addition to strong interannual variability in MLIE across the study area, we observed distinct spatial patterns in MLIE across the four regions within the study area (Figures 3 and 4). MLIE extends furthest from the coastline in the Amundsen Gulf region to a

maximum of ≈400 km and has the highest average MLIE decline over the entire study duration (−81%). North Banks Island region also has MLIE which extends far out from the northern coastlines at a maximum of ≈200 km; however, this region has the lowest average MLIE % decline over the 20-year period (−14%) in MLIE distance from coastline. The Mackenzie Delta and West Banks Island regions had similar maximum extents at ≈120 km and ≈80 km and average declines of 48% and 60%, respectively, over this time.

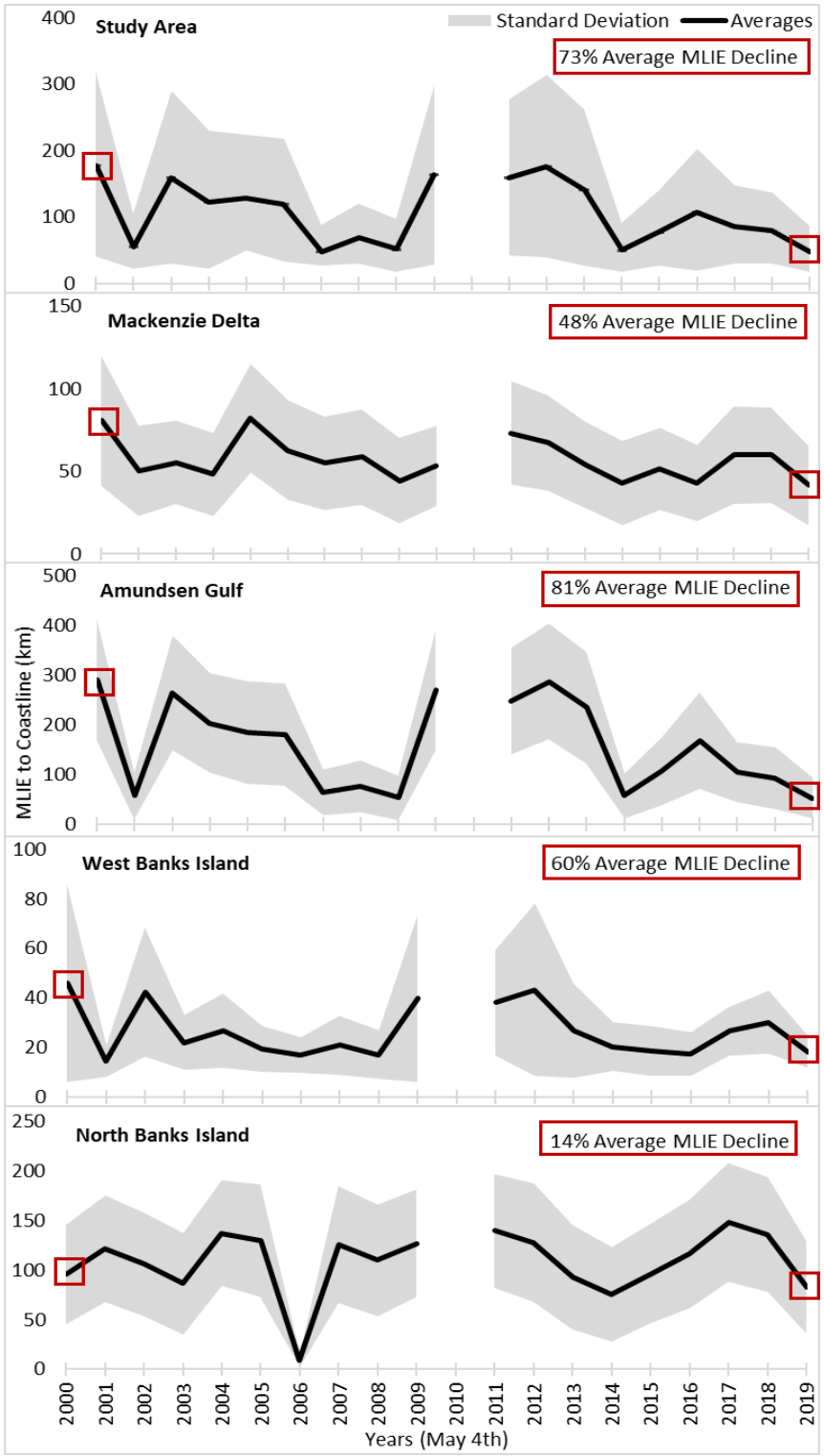

Figure 3. Average MLIE distance perpendicular from the coastline, on the 125th Day (4 May) from 2000 to 2019 per year, across the study area and regions. Red boxes outline the average % distance

from coastline change in MLIE when comparing the years 2000 and 2019 directly, however the fluctuations of individual years are still identified. Greyed outline shows the variability (standard deviation) from the average MLIE across the study area and regions. Note this variability is not error; rather, it simply reflects natural variability in landfast ice position along the coastline.

These spatial variations in MLIE distance from the coastline across the four regions show the importance of assessing site-specific landfast ice processes. If the study area average comparing the years 2000 and 2019 directly (73%) was applied to the North Banks Island region (14%), it would significantly overestimate MLIE decline by 59% over the two decades, a five-fold increase in MLIE decline. Whereas, if the study area average MLIE decline in distance from the coastline was applied to the Amundsen Gulf region, this would underestimate MLIE decline by 8%. Overall, it is clear averaged values mask critical variations across the four regions observed within this study area.

Table 1. MLIE pattern variability with rich or poor periods, shown in positive or negative relative % change compared to the average MLIE throughout the study period for the entire study area and each of the four regions. MLIE poor periods are highlighted in grey.

	MLIE % Variability Compared to Average MLIE Over Study Period				
Year	**Study Area**	**Mackenzie Delta**	**Amundsen Gulf**	**West Banks Island**	**North Banks Island**
2000	67	41	84	73	−12
2001	−47	−12	−64	−45	12
2002	50	−3	67	59	−3
2003	16	−15	29	−17	−20
2004	20	44	16	1	26
2005	12	10	14	−27	20
2006	−54	−4	−59	−37	−92
2007	−36	3	−52	−22	16
2008	−51	−23	−66	−36	1
2009	54	−7	71	49	17
2010	-	-	-	-	-
2011	50	28	57	43	29
2012	66	18	82	63	18
2013	32	−5	49	1	−15
2014	−53	−25	−64	−23	−30
2015	−27	−10	−32	−30	−11
2016	1	−25	7	−35	7
2017	−19	5	−33	0	36
2018	−26	5	−41	14	25
2019	−55	−27	−67	−31	−24

3.2. Static Controls—Topographic Setting and Bathymetry

Distinct spatial variations in MLIE occurred across the study area in relation to topographic setting and bathymetry. For example, in the Mackenzie Delta region, MLIE varied from west to east across the deltaic environment and islands between 2000 and 2019 (Figure 4A). MLIE across all years were more variable to the west of the delta towards Herschel Island, where the main river channel meets the Beaufort Sea and forms deeper water, with a maximum interannual MLIE distance from coastline variation of ≈100 km present (Figure 4B). This is contrasted with the relatively uniform interannual MLIE positions to the northeast of the delta. There is less (≈50 km) variability in interannual MLIE coinciding with the shallower bathymetry further northeast along the coastline surrounding the Tuktoyaktuk Peninsula. Similarly, MLIE remained close to the coastline over the past two decades across the West Banks Island region, not extending further than ≈50 km into the

Beaufort Sea. The MLIEs in both the Mackenzie Delta and West Banks Island regions were strongly correlated with the 30 m isobath, with most years remaining at or constrained within the area defined by the 30 m isobath (Figure 5). The MLIE spatial pattern remained similar along the cliff coastline of West Banks Island, until the Beaufort Sea reached an opening of where it became less constrained in the deep bathymetry of the North Banks Island region (Figure 4). Both the North Banks Island and Amundsen Gulf regions did not show a statistically significant bathymetric control, likely due to both regions having deep sea floors with steep seabed drops. Moreover, the spatial pattern in the Amundsen Gulf region was unique compared to other regions. It displayed the largest MLIE distance from the coastline across the Northwest Canadian Arctic (Figure 4), extending ≈500 km from the southeastern coastline of the gulf to its maximum at the mouth. This high MLIE distance from the coastline coincides with a complex mix of topographic settings encircling the gulf. For example, there are four observable clusters within the Amundsen Gulf region, with one at the mouth of the gulf, one at the back of the gulf, and then two in the center. One of the central clusters (Figure 4A(i)) is between two pinch points, where two headlands create a topographic narrowing in the gulf. The second central cluster of MLIE (Figure 4A(ii)) is south of the large channel, opening into the gulf on the east coast of Banks Island.

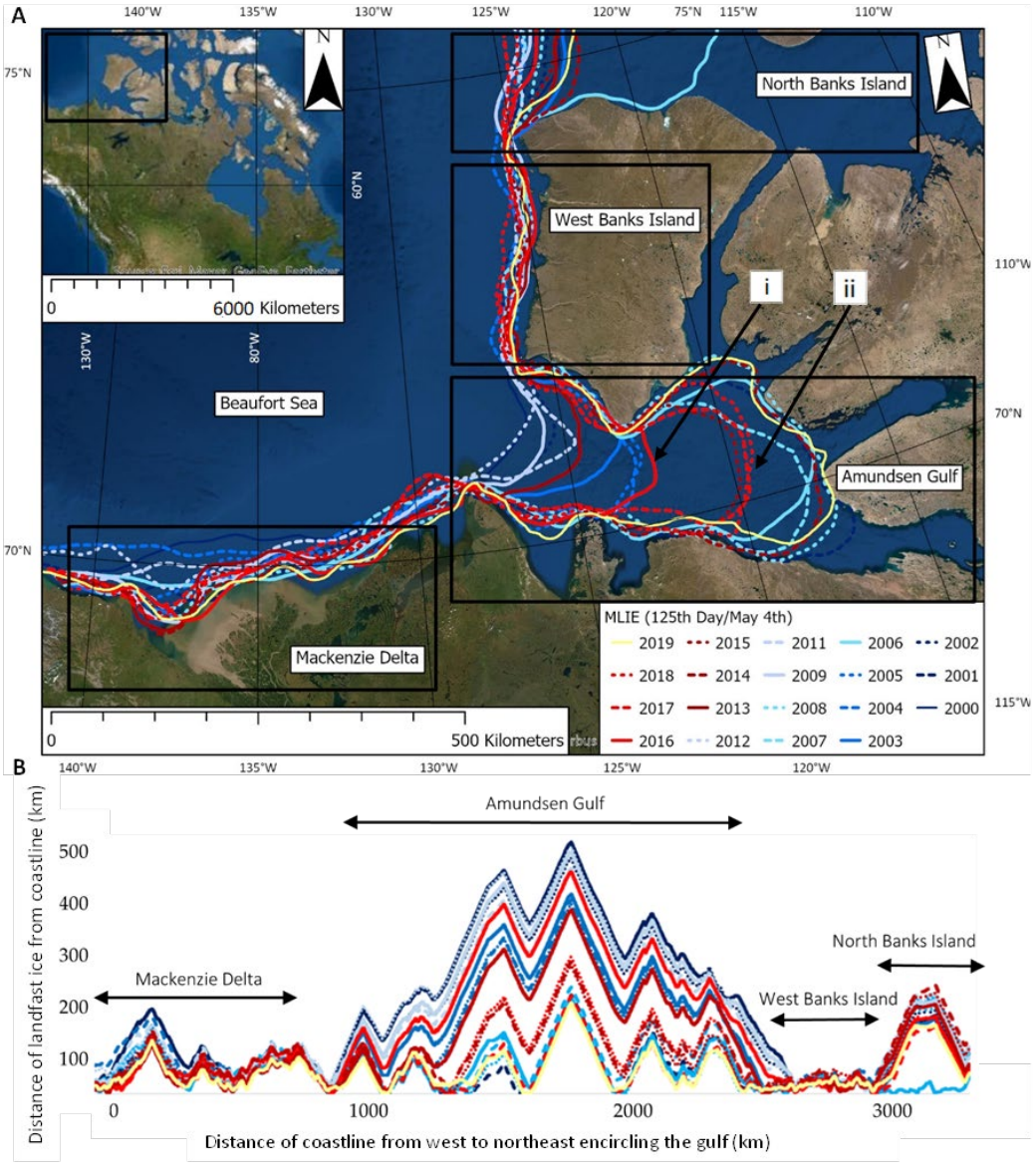

Figure 4. (**A**) The visual MLIE position per 4th of May from 2000 to 2019 across the study area and four regions outlined in black boxes. Both (i) and (ii) represent two of the four clusters discussed. (**B**) The distance in km of MLIE perpendicular from the coastline across the study area and four regions outlined with black arrows.

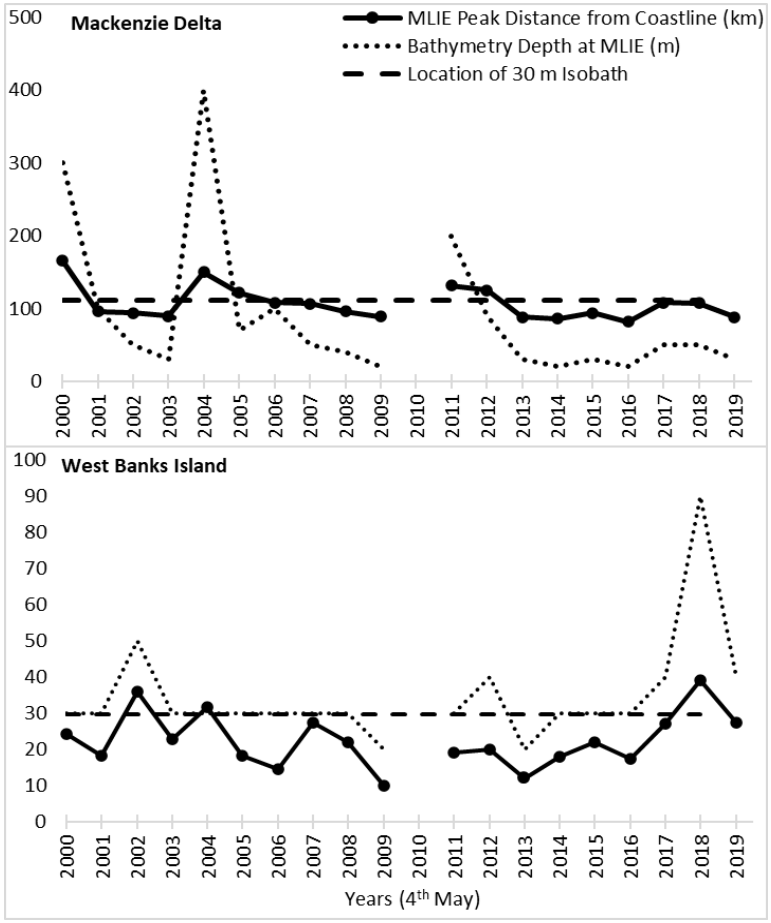

Figure 5. Bathymetric control at Mackenzie Delta and West Banks Island (refer to Figure 1 for bathymetry). Line plots show annual sequencing of MLIE distance from coastline with bathymetry depth achieved, relative to 30 m isobath. Key shows distance (*y*-axis) of both MLIE and bathymetry depth.

3.3. Dynamic Controls—Storm Duration, Mean Air Temperature, Freezing and Thawing Degree Day Occurrence

This study found no statistically significant relationship between MLIE and storminess or air temperature. Specifically, total duration of storm conditions, storm conditions directed toward MLIE edge, MAT, FDD, and TDD, did not show a strong direct control on interannual MLIE across the Northwest Canadian Arctic study area or within any of the four regions when analysed over 1, 3, and 12-month periods (data available on request).

To examine the potential for storm impacts on the MLIE prior to mapping, study area and regional MLIE averages for the preceding 3-month period were studied (Figure 6). No significant relationships between storm duration and the MLIE were identified. Particularly, across the study area, the interannual variability of both total storm duration and average MLIE distance from the coastline appeared to have an inverse relationship (Figure 6). In the Mackenzie Delta region, total storm duration varied with no consistent pattern until 2014 and then underwent a marked rise until 2019, equating to a 350% (90 h) increase in annual storm conditions (Figure 6). Even with a 5-year increase in cumulative storm duration, no change in average MLIE was observed. Additionally, no significant

relationships between MLIE and increased storm duration were found when only storms with prevailing directions facing the landfast ice edge were included (Figure 6). Notably, westerly storms impacting the MLIE at the mouth of the Amundsen Gulf region and in the North Banks Island region exerted no discernible control over MLIE.

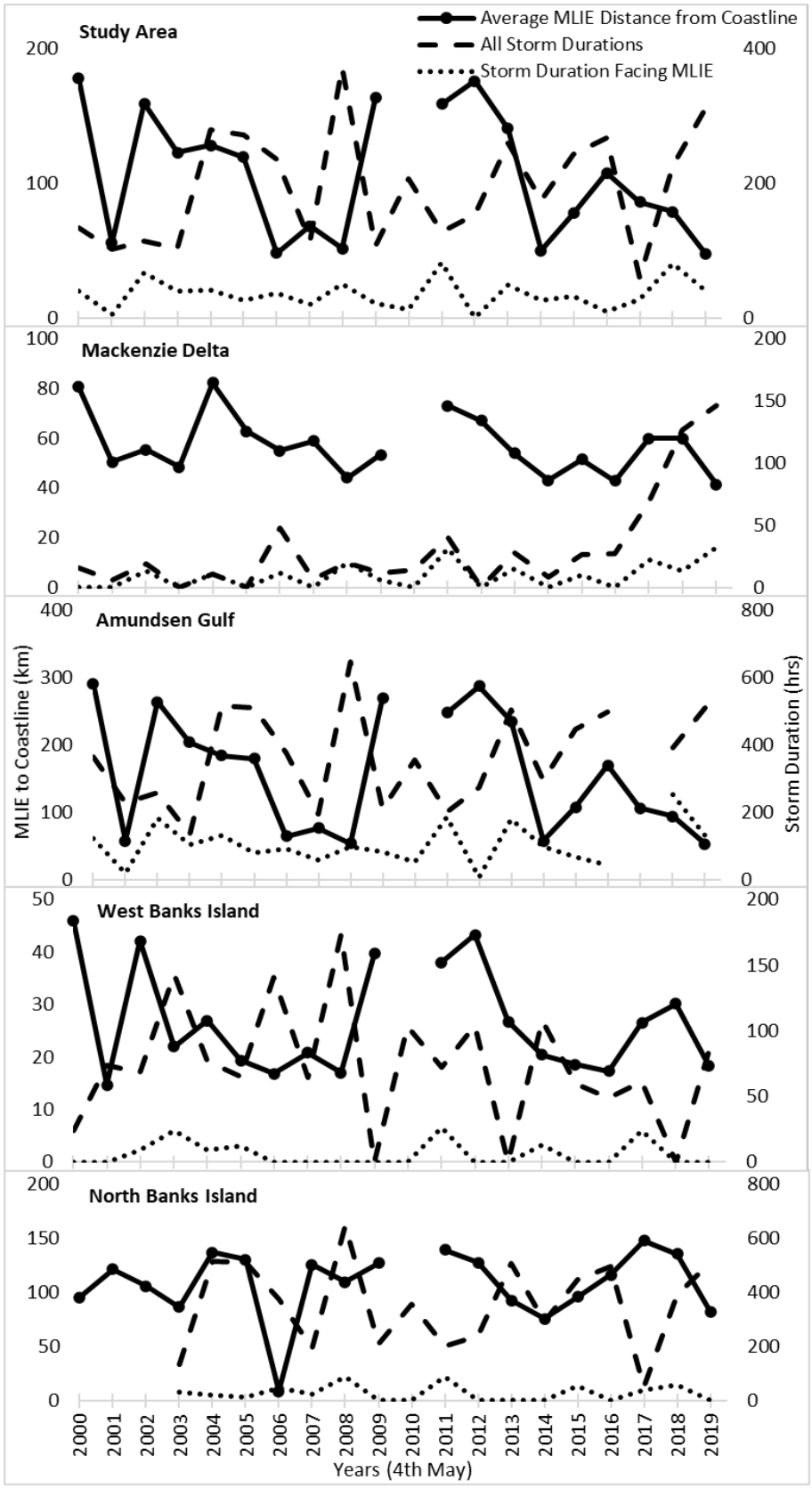

Figure 6. Average MLIE distance from the coastline, all storm duration, and storm duration facing the MLIE edge averaged for the preceding 3 months across the Northwest Canadian Arctic study area and each of the four regions from 2000 to 2019 is shown.

These data demonstrate that storm direction, duration, scale, and timeframe do not have a clear and inverse relationship with MLIE. No statistically significant relationships between MLIE and MAT, FDD, and TDD across all scales and time frames were recorded. For example, one of the highest MAT values occurred at West Banks Island in 2001, however the MLIE reached one of its furthest distances from the coastline. While MAT shows a consistent pattern across the study period, with colder temperatures found further North, across the Northwest Canadian Arctic, there is no significant correlation with MLIE. Overall, we could identify no significant influence of the dynamic controls on the MLIE at any scale or timeframe tested. These data demonstrate the complex nature of landfast ice, which does not show similar patterns of control exhibited by other broad composite sea ice studies, which comprise of and do not distinguish between pack ice, drifting ice, and landfast ice [57–59].

4. Discussion

4.1. Importance of Differentiating between Sea Ice and Landfast Ice

Numerous Arctic Sea ice studies have shown concerning data regarding past and future declines in sea ice extent to climate changes [57,60–64]. However, there is a lack of differentiation between sea ice and landfast ice patterns, variability, and trends across the Northwest Canadian Arctic, which accounts for 30% of all Arctic landfast ice [1,2]. There is also a lack of analyses of landfast ice influences and controls compared to drifting sea ice or pack ice, resulting in assumptions and inferences about potential impacts and future process changes. Here, we have shown how landfast ice extent fundamentally differs from known composite sea ice extent patterns and controls, which comprise of and do not distinguish between pack ice, drifting ice, and landfast ice.

We appear to find an interannual landfast ice 'memory' resulting in a 5–8-year cycle from rich to poor MLIE periods. Accounting for these cycles, we found no discernible trend in MLIE decline over time, whereas previous studies have shown trends in declining sea ice (particularly pack ice and drifting ice) since the satellite era began [60–62,65]. This continuity of cycling recorded has not been found in previous composite sea ice studies [57], thus showing a critical difference between landfast ice and other forms of sea ice. Another difference is our landfast ice extent data reveal extreme interannual variability, significantly beyond that recorded in sea ice extent studies, particularly across this region of the Arctic [57–59]. For example, we found the average MLIE difference from 2000 to 2001 across the study area decreased by ≈150 km and then increased the following year by ≈100 km. This demonstrates large landfast ice fluctuations over yearly timeframes. A recent sea ice study found variations in the Canadian Arctic sea ice extent, but these were less pronounced due to the decadal and multi-year averages used [59], suggesting the temporal resolution of the data may be a limiting factor on other sea ice studies too, and thus lose annual resolution of the high and low extents. Therefore, using composite sea ice patterns, variability, and trends to interpret landfast ice changes could potentially lead to misrepresentations and significant impacts for communities and northern stakeholders.

Sea ice extent has previously been determined to be strongly controlled by dynamic climatic processes [56–59,66], but such linkages are not evident in the MLIE patterns presented here. From previous sea ice studies [66,67], storm impacts (such as wind-blown waves) might be expected to have a strong relationship on MLIE distance from coastline. For example, in the summer of 2012, the 'Great Arctic Storm' significantly reduced Arctic Sea ice extent for the following year in 2013. However, we found no signal of the 2012 'Great Arctic Storm' in our storm data for the Mackenzie Delta, Amundsen Gulf, and West Banks Island regions. There was a weak signal of this storm recorded in the most northern region of North Banks Island. However, even within the North Banks Island region, we

still did not find a significant control from the previous 12 months total storm duration on MLIE distance from the coastline. A recent sea ice study found control from oceanographic factors linked with previous wind perturbations (both positive and negative phases of the Beaufort High, Arctic Oscillation, and Arctic Dipole Anomaly) [68]. These previous wind perturbations (signals) found within the oceanographic controls tested, helped to explain patterns of sea ice drift, thickness, concentration, and deformation rates. We are yet to find any previous signals, such as the previous wind perturbations above, within a dynamic control on patterns of MLIE, and more specifically linking to the 5–8-year memory cycling patterns we have found, thus opening new avenues for exploratory research.

Additionally, sea ice extent has been directly linked to temperature in previous research across the Arctic [57,69–72], however no air temperature control was found when tested against MLIE distance from coastline. Instead, our new landfast ice data identify the potential for catastrophic annual declines in MLIE that are poorly explained by dynamic controls already known to influence sea ice extremes. Other landfast ice components, such as ice thickness and breakup timing, have found a correlation with dynamic controls. For example, previous field-based research using sparse, widespread sites identified landfast ice thickness to be largely driven by interannual variations of air temperature [73]. However, more recent modelling has found the correlation to be present but significantly weaker than first recorded [74]. Previous research has also identified that spring air temperature has a first order control on spring breakup timing of landfast ice surrounding communities across the Canadian Arctic [9]. Collectively, this previous work and our new results emphasize that different landfast ice components, such as thickness, breakup timing, and maximum extent, respond differently to the same dynamic environmental controls. Further work is needed to explore other dynamic controls on MLIE including but not limited to oceanographic controls (such as wave height and strength), increased winter precipitation, saltwater and freshwater mixing, Beaufort Gyre strength, and the ice state (such as the degree of 'rotten' ice). Our data have opened exciting new avenues of research for dynamic controls to be tested with a focus on memory signals and the 5–8-year cycling of MLIE.

Our results do indicate that static features such as coastal setting and bathymetry have a statistically significant control on MLIE; the sedentary nature of landfast ice makes it distinct from drifting sea ice. For example, the presence or absence of islands, headlands, straits, and the location of the 30 m isobath exert discernible control on the mean location of landfast ice extent, although these factors do not seem to influence changes in MLIE over time. Therefore, it is important to account for topographic and bathymetric setting in order to determine the true sensitivity of landfast ice patterns and processes to climatic changes.

4.2. Inuit Community Reliance on and Vulnerability to Landfast Ice Variability

Future climate impacts on landfast ice variability are expected to be magnified, although in ways that are poorly understood across the Beaufort Sea region [29,75]. The interannual variability and lack of a discernible trend in MLIE we have recorded causes growing concern for increased vulnerability, particularly across the Inuvialuit Settlement Region (ISR), as we are yet to discover a clear dynamic control. Communities within the ISR rely on the semi-permanent transport routes over landfast ice to access hunting, fishing, trapping, gathering, and travel between communities and to visit culturally significant sites [29,76]. Many studies have recorded changes that have compromised food security and highlighted the potentially fatal consequences of unpredictable and variable landfast ice [29,38,77]. Within this region, for 7–8 months of the year, the landfast ice is a part of the landscape and is an important component to the Inuit way of life. However, the specific concerns and vulnerabilities are typically dependent on the specific community and their interaction with the landfast ice. For example, although these semi-permanent transport routes, such as ice roads, have become increasingly unreliable [77], recent

research has found that transport issues over these once predictable ice trails is of varying significance, as some communities have reported developing new trails and alternating transport modes to combat these changes [36,75,78]. This is evident in the community of Ulukhaktok, as they reported an increase in hunters switching to automated terrain vehicles (ATV's) to hunt caribou and switching away from trails they now consider a risk [36]. Another example of critical changes surrounding communities due to changes in the landfast ice zone is the permanent closure of the Inuvik-Tuktoyaktuk ice road in 2017. This was in part due to the more noticeable and increasing interannual variability of cracks and flooded patches making the once commonly used ice road now unsafe to use [36,75,78]. Although, the creation of the Inuvik-Tuktoyaktuk Highway has now created a permanent connection [79]. These adaptations demonstrate the innovative ways and transformative approaches that the Inuit population have undertaken to sustain their way of life in the North [76].

It is important to assess the main concern of the specific community in order to effectively improve resilience to landfast ice changes. For example, in Sachs Harbour and Ulukhaktok they are close to open water (Figure 4) and so whether landfast ice extent in the gulf is related to common hunting grounds and over ice community transportation routes are ice free or not, is potentially the most important factor. In contrast, at Tuktoyaktuk and Paulatuk, the emphasis may shift to landfast ice properties such as thickness instead of just extent, due to their use of ice roads for safety. Overall, a key aspect to understanding the local impacts of the widescale variations identified here should be on connecting Inuit knowledge and specific datasets to improve future predictability and resilience to landfast ice variability [80].

4.3. Appropriate Spatiotemporal Metrics and Scales for Landfast Ice Studies

Our data clearly indicate that landfast ice requires specific consideration rather than as a component of composite sea ice studies, in agreement with previous studies [5,9,81]. For example, many sea ice studies use fixed averages when providing change over time and space. However, a fixed average does not adequately reflect the complex response of landfast ice regional distinctiveness, influenced by coastal topographic and bathymetric setting. For instance, within the Mackenzie Delta there was large spatial variation from more constrained MLIEs to the east with its many islands and shallow bathymetry of the Tuktoyaktuk Peninsula than to the deeper estuary area to the west (Figure 4A). The specific detail of the metric and scale is dependent upon the need of the user. If a community or northern stakeholder is reliant upon landfast ice in a specific area, then the spatial and temporal resolutions achieved by this analysis have particular value and provide a new perspective for critical decision making. Temporally, data on interannual variability is more crucial to a community whereas a decadal average would help to refine the changing long-term exposure of coastal sites to marine erosion.

Previous research has stated that automation processes are key to reduce human digitization error even when a skilled analyst is used [1,82]. Following the approach presented here, there is significant new potential to automate the mapping process of free, frequent, satellite imagery. Automating the ice edge mapping process could allow scale to be adapted based on the requirement of the user, for example at a pan-arctic, regional, subregional, and local process level, and also allow local community users to integrate their in-depth knowledge with current MLIE outputs.

5. Conclusions

We have presented new analyses of freely available satellite data to map the maximum extent of landfast ice across the Northwest Canadian Arctic over a 20-year period. Interannual landfast ice patterns, variability, and trends demonstrate the need to monitor and analyze landfast ice as a specific component and not simply inferred from sea ice patterns. Landfast ice has undergone significant interannual fluctuations, with 5–8-year cycling of landfast ice rich and poor periods but with no discernible trend in MLIE decline.

This progressive dynamism was superimposed on spatially distinct static controls such as coastal setting and bathymetry on the severity of the landfast ice fluctuations. The ability to evaluate year-on-year MLIE variations helps address a pressing need for the interpretation and prediction of future landfast ice impacts directly on communities, transport, and ecology and indirectly on coastal erosion processes using the appropriate metric and scale.

Author Contributions: Conceptualization, E.E.W., S.W.C., P.J.M., D.W. and M.L.; methodology, E.E.W., S.W.C., P.J.M., D.W., P.F. and M.L.; software, E.E.W., S.W.C., P.J.M., P.F. and M.L.; validation, E.E.W., P.J.M. and M.L.; formal analysis, E.E.W., P.J.M. and M.L.; investigation, E.E.W., P.J.M. and M.L.; resources, E.E.W., S.W.C., P.J.M., D.W., P.F. and M.L.; data curation, E.E.W., S.W.C., P.J.M., D.W., P.F. and M.L.; writing—original draft preparation, E.E.W.; writing—review and editing, E.E.W., S.W.C., P.J.M., D.W. and M.L.; visualization, E.E.W., S.W.C., P.J.M., D.W. and M.L.; supervision, E.E.W., P.J.M., D.W. and M.L.; project administration, E.E.W., P.J.M. and M.L.; funding acquisition, E.E.W., S.W.C., P.J.M., D.W. and M.L. All authors have read and agreed to the published version of the manuscript.

Funding: This research was funded by Natural Environment Research Council, Grant Number: OP20241.

Data Availability Statement: All data required to evaluate the conclusions made in this paper are present within this paper. Additional data may be requested from the authors. All data can also be accessed online from the following data centers: MOD09GQ and MOD09GA data from https://lpdaac. usgs.gov, maintained by the NASA EOSDIS LP DAAC at the USGS/EROS Center, Sioux Falls, South Dakota; Weather data pertaining to storm frequency, duration, and mean air temperature from the Environment and Climate Change Canada (ECCC) were available from the stations proximal to the MLIE position tested in each region from https://weather.gc.ca (accessed on 12 May 2021) using the R package weathercan https://github.com/ropensci/weathercan (accessed on 12 May 2021).

Acknowledgments: The authors gratefully acknowledge the NERC UK-Canada Bursary funding scheme and the NERC ONE Planet project (OP20241) that funded this research. S.C. gratefully acknowledges funding from NSF Navigating the New Arctic (NNA) grant #1836573 managed by R. Delgado.

Conflicts of Interest: The authors declare no conflict of interest.

References

1. Li, Z.; Zhao, J.; Su, J.; Li, C.; Cheng, B.; Hui, F.; Yang, Q.; Shi, L. Spatial and Temporal Variations in the Extent and Thickness of Arctic Landfast Ice. *Remote Sens.* **2020**, *12*, 64. https://doi.org/10.3390/RS12010064.
2. Maslanik, J.; Stroeve, J.; Fowler, C.; Emery, W. Distribution and trends in Arctic sea ice age through spring 2011. *Geophys. Res. Lett.* **2011**, *38*, L13502. https://doi.org/10.1029/2011GL047735.
3. Barry, R.G.; Moritz, R.E.; Rogers, J.C. The fast ice regimes of the Beaufort and Chukchi Sea coasts, Alaska. *Cold Reg. Sci. Technol.* **1979**, *1*, 129–152. https://doi.org/10.1016/0165-232X(79)90006-5.
4. Petrich, C.; Eicken, H.; Zhang, J.; Krieger, J.; Fukamachi, Y.; Ohshima, K.I. Coastal landfast sea ice decay and breakup in northern Alaska: Key processes and seasonal prediction. *J. Geophys. Res. Ocean* **2012**, *117*, C02003. https://doi.org/10.1029/2011JC007339.
5. Mahoney, A.R.; Eicken, H.; Gaylord, A.G.; Gens, R. Landfast sea ice extent in the Chukchi and Beaufort Seas: The annual cycle and decadal variability. *Cold Reg. Sci. Technol.* **2014**, *103*, 41–56. https://doi.org/10.1016/J.COLDREGIONS.2014.03.003.
6. Lantuit, H.; Pollard, W.H. Fifty years of coastal erosion and retrogressive thaw slump activity on Herschel Island, southern Beaufort Sea, Yukon Territory, Canada. *Geomorphology* **2008**, *95*, 84–102. https://doi.org/10.1016/J.GEOMORPH.2006.07.040.
7. Yu, Y.; Stern, H.; Fowler, C.; Fetterer, F.; Maslanik, J. Interannual Variability of Arctic Landfast Ice between 1976 and 2007. *J. Clim.* **2014**, *27*, 227–243. https://doi.org/10.1175/JCLI-D-13-00178.1.
8. Lemieux, J.-F.; Tremblay, L.B.; Dupont, F.; Plante, M.; Smith, G.C.; Dumont, D. A basal stress parameterization for modeling landfast ice. *J. Geophys. Res. Ocean* **2015**, *120*, 3157–3173. https://doi.org/10.1002/2014JC010678.
9. Cooley, S.W.; Ryan, J.C.; Smith, L.C.; Horvat, C.; Pearson, B.; Dale, B.; Lynch, A.H. Coldest Canadian Arctic communities face greatest reductions in shorefast sea ice. *Nat. Clim. Chang.* **2020**, *10*, 533–538. https://doi.org/10.1038/s41558-020-0757-5.
10. Dammann, D.O.; Eriksson, L.E.B.; Mahoney, A.R.; Eicken, H.; Meyer, F.J. Mapping pan-Arctic landfast sea ice stability using Sentinel-1 interferometry. *Cryosphere* **2019**, *13*, 557–577. https://doi.org/10.5194/TC-13-557-2019.
11. Jensen, D.; Mahoney, A.; Resler, L. The annual cycle of landfast ice in the eastern Bering Sea. *Cold Reg. Sci. Technol.* **2020**, *174*, 103059. https://doi.org/10.1016/J.COLDREGIONS.2020.103059.

12. Overeem, I.; Anderson, R.S.; Wobus, C.W.; Clow, G.D.; Urban, F.E.; Matell, N. Sea ice loss enhances wave action at the Arctic coast. *Geophys. Res. Lett.* **2011**, *38*, L17503. https://doi.org/10.1029/2011GL048681.
13. Markus, T.; Stroeve, J.C.; Miller, J. Recent changes in Arctic sea ice melt onset, freezeup, and melt season length. *J. Geophys. Res.* **2009**, *114*, C12024. https://doi.org/10.1029/2009JC005436.
14. Divine, D.V.; Korsnes, R.; Makshtas, A.P. Temporal and spatial variation of shore-fast ice in the Kara Sea. *Cont. Shelf Res.* **2004**, *24*, 1717–1736. https://doi.org/10.1016/J.CSR.2004.05.010.
15. Nghiem, S.V.; Hall, D.K.; Rigor, I.G.; Li, P.; Neumann, G. Effects of Mackenzie River discharge and bathymetry on sea ice in the Beaufort Sea. *Geophys. Res. Lett.* **2014**, *41*, 873–879. https://doi.org/10.1002/2013GL058956.
16. Shestov, A.S.; Marchenko, A.V. Thermodynamic consolidation of ice ridge keels in water at varying freezing points. *Cold Reg. Sci. Technol.* **2016**, *121*, 1–10. https://doi.org/10.1016/J.COLDREGIONS.2015.09.015.
17. Mahoney, A.; Eicken, H.; Gaylord, A.G.; Shapiro, L. Alaska landfast sea ice: Links with bathymetry and atmospheric circulation. *J. Geophys. Res. Ocean* **2007**, *112*, C02001. https://doi.org/10.1029/2006JC003559.
18. Trishchenko, A.P.; Luo, Y. Landfast Ice Mapping Using MODIS Clear-Sky Composites: Application for the Banks Island Coastline in Beaufort Sea and Comparison with Canadian Ice Service Data. *Can. J. Remote Sens.* **2021**, *47*, 143–158. https://doi.org/10.1080/07038992.2021.1909466.
19. Haas, C.; Dierking, W.; Busche, T.; Hölemann, J. Envisat ASAR monitoring of polynya processes and sea ice production in the Laptev Sea. In Proceedings of the 2004 Envisat & ERS Symposium (ESA SP-572), Salzburg, Austria, 6–10 September 2004.
20. Wadhams, P. *Ice in the Ocean*; CRC Press: London, UK, 2014. https://doi.org/10.1201/9781482283082.
21. Candlish, L.M.; Iacozza, J.; Lukovich, J.V.; Horton, B.; Barber, D.G. Sea ice climatology in the Canadian Western Arctic: Thermodynamic versus dynamic controls. *Int. J. Climatol.* **2015**, *35*, 1867–1880. https://doi.org/10.1002/JOC.4094.
22. Lemieux, J.-F.; Lei, J.; Dupont, F.; Roy, F.; Losch, M.; Lique, C.; Laliberté, F. The Impact of Tides on Simulated Landfast Ice in a Pan-Arctic Ice-Ocean Model. *J. Geophys. Res. Ocean* **2018**, *123*, 7747–7762. https://doi.org/10.1029/2018JC014080.
23. Frederick, J.M.; Thomas, M.A.; Bull, D.L.; Jones, C.A.; Roberts, J.D. *The Arctic Coastal Erosion Problem*; U.S. Department of Energy, Office of Scientific and Technical Information: Washington, DC, USA, 2016. https://doi.org/10.2172/1431492.
24. Stewart, E.J.; Howell, S.E.L.; Draper, D.; Yackel, J.; Tivy, A. Sea Ice in Canada's Arctic: Implications for Cruise Tourism. *ARCTIC* **2007**, *60*, 370–380. https://doi.org/10.14430/ARCTIC194.
25. Gignac, C.; Bernier, M.; Chokmani, K.; Poulin, J. IceMap250—Automatic 250 m Sea Ice Extent Mapping Using MODIS Data. *Remote Sens.* **2017**, *9*, 70. https://doi.org/10.3390/rs9010070.
26. Jones, B.M.; Arp, C.D.; Jorgenson, M.T.; Hinkel, K.M.; Schmutz, J.A.; Flint, P.L. Increase in the rate and uniformity of coastline erosion in Arctic Alaska. *Geophys. Res. Lett.* **2009**, *36*, L03503. https://doi.org/10.1029/2008GL036205.
27. Overduin, P.P.; Strzelecki, M.C.; Grigoriev, M.N.; Couture, N.; Lantuit, H.; St-Hilaire-Gravel, D.; Günther, F.; Wetterich, S. Coastal changes in the Arctic. *Geol. Soc. London Spec. Publ.* **2014**, *388*, 103–129. https://doi.org/10.1144/SP388.13.
28. Croasdale, K.; Frederking, R.; Jordaan, I.; Noble, P. *Engineering in Canada's Northern Oceans; Research and Strategies for Development—A Report for the Canadian Academy of Engineering*; Canadian Academy of Engineering: Ottawa, ON, Canada, 2016; ISBN 9781928194026.
29. Ford, J.D.; Clark, D.; Pearce, T.; Berrang-Ford, L.; Copland, L.; Dawson, J.; New, M.; Harper, S.L. Changing access to ice, land and water in Arctic communities. *Nat. Clim. Chang.* **2019**, *9*, 335–339. https://doi.org/10.1038/s41558-019-0435-7.
30. Barber, D.G.M.J. The International Polar Year (IPY) Circumpolar Flaw Lead (CFL) System Study: A Focus on Fast Ice Edge Systems—NASA/ADS. Available online: https://ui.adsabs.harvard.edu/abs/2009AGUFM.C53B..04B/abstract (accessed on 29 October 2021).
31. Laidre, K.L.; Stirling, I.; Lowry, L.F.; Wiig, Ø.; Heide-Jørgensen, M.P.; Ferguson, S.H. Quantifying the sensitivity of arctic marine mammals to climate-induced habitat change. *Ecol. Appl.* **2008**, *18*, S97–S125. https://doi.org/10.1890/06-0546.1.
32. Burn, C.R. *Herschel Island (Qikiqtaryuk), Yukon's Arctic Island*; Springer: Berlin/Heidelberg, Germany, 2017; pp. 335–348. https://doi.org/10.1007/978-3-319-44595-3_24.
33. Nagy, M. Reinterpreting the First Human Occupations of Ivujivik (Nunavik, Canada). *Arct. Anthropol.* **2018**, *55*, 17–43. https://doi.org/10.3368/aa.55.2.17.
34. Burek, K.A.; Gulland, F.M.D.; O'Hara, T.M. Effects of climate change on arctic marine mammal health. *Ecol. Appl.* **2008**, *18*, S126–S134. https://doi.org/10.1890/06-0553.1.
35. Kovacs, K. *Circumpolar Ringed Seal (Pusa hispida) Monitoring: CAFF's Ringed Seal Monitoring Network*; Rapportserie 143; Norsk Polar Institute: Tromsø, Norway, 2014; 48p.
36. Fawcett, D.; Pearce, T.; Notaina, R.; Ford, J.D.; Collings, P. Inuit adaptability to changing environmental conditions over an 11-year period in Ulukhaktok, Northwest Territories. *Polar Rec. (Gr. Brit)* **2018**, *54*, 119–132. https://doi.org/10.1017/S003224741800027X.
37. NWT Bureau of Statistics. 2018 Engaged in Traditional Activities. Available online: https://www.statsnwt.ca/Traditional%20Activities/ (accessed on 22 February 2021).
38. Dumas, J.A.; Flato, G.M.; Brown, R.D. Future Projections of Landfast Ice Thickness and Duration in the Canadian Arctic. *J. Clim.* **2006**, *19*, 5175–5189. https://doi.org/10.1175/JCLI3889.1.
39. Lim, M.; Whalen, D.; Martin, J.; Mann, P.J.; Hayes, S.; Fraser, P.; Berry, H.B.; Ouellette, D. Massive Ice Control on Permafrost Coast Erosion and Sensitivity. *Geophys. Res. Lett.* **2020**, *47*, e2020GL087917. https://doi.org/10.1029/2020GL087917.

40. Waseda, T.; Webb, A.; Sato, K.; Inoue, J.; Kohout, A.; Penrose, B.; Penrose, S. Correlated Increase of High Ocean Waves and Winds in the Ice-Free Waters of the Arctic Ocean. *Sci. Rep.* **2018**, *8*, 4489. https://doi.org/10.1038/s41598-018-22500-9.
41. Abbott, B.W.; Jones, J.B.; Godsey, S.E.; Larouche, J.R.; Bowden, W.B. Patterns and persistence of hydrologic carbon and nutrient export from collapsing upland permafrost. *Biogeosciences* **2015**, *12*, 3725–3740. https://doi.org/10.5194/BG-12-3725-2015.
42. Couture, N.J.; Irrgang, A.; Pollard, W.; Lantuit, H.; Fritz, M. Coastal Erosion of Permafrost Soils along the Yukon Coastal Plain and Fluxes of Organic Carbon to the Canadian Beaufort Sea. *J. Geophys. Res. Biogeosci.* **2018**, *123*, 406–422. https://doi.org/10.1002/2017JG004166.
43. Cunliffe, A.M.; Tanski, G.; Radosavljevic, B.; Palmer, W.F.; Sachs, T.; Lantuit, H.; Kerby, J.T.; Myers-Smith, I.H. Rapid retreat of permafrost coastline observed with aerial drone photogrammetry. *Cryosphere* **2019**, *13*, 1513–1528. https://doi.org/10.5194/tc-13-1513-2019.
44. Tanski, G.; Wagner, D.; Knoblauch, C.; Fritz, M.; Sachs, T.; Lantuit, H. Rapid CO_2 Release from Eroding Permafrost in Seawater. *Geophys. Res. Lett.* **2019**, *46*, 11244–11252. https://doi.org/10.1029/2019GL084303.
45. Turetsky, M.R.; Abbott, B.W.; Jones, M.C.; Walter Anthony, K.; Olefeldt, D.; Schuur, E.A.G.; Koven, C.; McGuire, A.D.; Grosse, G.; Kuhry, P.; et al. Permafrost collapse is accelerating carbon release. *Nature* **2019**, *569*, 32–34. https://doi.org/10.1038/d41586-019-01313-4.
46. Shokr, M.; Sinha, N.K. Sea Ice: Physics and Remote Sensing—Google Books. Available online: https://books.google.co.uk/books?hl=en&lr=&id=GnNuBwAAQBAJ&oi=fnd&pg=PR3&dq=+Sea+ice:+physics+and+remote+sensing+shokra+and+sinha+2015&ots=TZLDaYkeb2&sig=-BXbJeR73hovHOneUGcSGFMW-xs&redir_esc=y#v=onepage&q&f=false (accessed on 9 November 2021).
47. Drüe, C.; Heinemann, G. High-resolution maps of the sea-ice concentration from MODIS satellite data. *Geophys. Res. Lett.* **2004**, *31*, L20403. https://doi.org/10.1029/2004GL020808.
48. Rees, W.G. *Remote Sensing of Snow and Ice*, 1st ed.; GIS, Remote Sensing and Cartography: Boca Raton, FL, USA, 2006**.**
49. Su, H.; Wang, Y. Using MODIS data to estimate sea ice thickness in the Bohai Sea (China) in the 2009–2010 winter. *J. Geophys. Res. Ocean* **2012**, *117*, 10018. https://doi.org/10.1029/2012JC008251.
50. Su, H.; Wang, Y.; Xiao, J.; Li, L. Improving MODIS sea ice detectability using gray level co-occurrence matrix texture analysis method: A case study in the Bohai Sea. *ISPRS J. Photogramm. Remote Sens.* **2013**, *85*, 13–20. https://doi.org/10.1016/J.ISPRSJPRS.2013.07.010.
51. Cooley, S.W.; Pavelsky, T.M. Spatial and temporal patterns in Arctic river ice breakup revealed by automated ice detection from MODIS imagery. *Remote Sens. Environ.* **2016**, *175*, 310–322. https://doi.org/10.1016/J.RSE.2016.01.004.
52. Trishchenko, A.P.; Kostylev, V.; Luo, Y.; Ungureanu, C.; Whalen, D.; Li, J. Landfast ice properties over the Beaufort Sea region in 2000-2019 from MODIS and Canadian Ice Service data. *Can. J. Earth Sci.* **2021**, *99*, 1–19. https://doi.org/10.1139/cjes-2021-0011.
53. Grid, G. GEBCO_2021 Grid. Available online: https://www.gebco.net/data_and_products/gridded_bathymetry_data/gebco_2021/?msclkid=80d07261b1ba11eca8680daf2522feb1 (accessed on 12 December 2021).
54. MacClenahan, P.; McKenna, J.; Cooper, J.A.G.; O'Kane, B. Identification of highest magnitude coastal storm events over Western Ireland on the basis of wind speed and duration thresholds. *Int. J. Climatol.* **2001**, *21*, 829–842. https://doi.org/10.1002/joc.666.
55. Hudak, D.R.; Young, J.M.C. Storm climatology of the Southern Beaufort sea. *Atmos.-Ocean* **2002**, *40*, 145–158. https://doi.org/10.3137/ao.400205.
56. Atkinson, D.E. Observed storminess patterns and trends in the circum-Arctic coastal regime. *Geo-Mar. Lett.* **2005**, *25*, 98–109. https://doi.org/10.1007/s00367-004-0191-0.
57. Serreze, M.C.; Meier, W.N. The Arctic's sea ice cover: Trends, variability, predictability, and comparisons to the Antarctic. *Ann. N. Y. Acad. Sci.* **2019**, *1436*, 36–53. https://doi.org/10.1111/nyas.13856.
58. Stroeve, J.; Notz, D. Changing state of Arctic sea ice across all seasons. *Environ. Res. Lett.* **2018**, *13*, 103001. https://doi.org/10.1088/1748-9326/aade56.
59. Cavalieri, D.J.; Parkinson, C.L. Arctic sea ice variability and trends, 1979–2010. *Cryosphere* **2012**, *6*, 881–889. https://doi.org/10.5194/tc-6-881-2012.
60. Parkinson, C.L.; Cavalieri, D.J.; Gloersen, P.; Zwally, H.J.; Comiso, J.C. Arctic sea ice extents, areas, and trends, 1978–1996. *J. Geophys. Res. Ocean* **1999**, *104*, 20837–20856. https://doi.org/10.1029/1999JC900082.
61. Vinnikov, K.Y.; Cavalieri, D.J.; Parkinson, C.L. A model assessment of satellite observed trends in polar sea ice extents. *Geophys. Res. Lett.* **2006**, *33*, L05704. https://doi.org/10.1029/2005GL025282.
62. Meier, W.N.; Stroeve, J.; Fetterer, F. Whither Arctic sea ice? A clear signal of decline regionally, seasonally and extending beyond the satellite record. *Ann. Glaciol.* **2007**, *46*, 428–434. https://doi.org/10.3189/172756407782871170.
63. Parkinson, C.L.; Cavalieri, D.J. Arctic sea ice variability and trends, 1979–2006. *J. Geophys. Res. Ocean* **2008**, *113*, C07003. https://doi.org/10.1029/2007JC004558.
64. Stroeve, J.; Holland, M.M.; Meier, W.; Scambos, T.; Serreze, M. Arctic sea ice decline: Faster than forecast. *Geophys. Res. Lett.* **2007**, *34*, L09501. https://doi.org/10.1029/2007GL029703.
65. Comiso, J.C.; Parkinson, C.L.; Gersten, R.; Stock, L. Accelerated decline in the Arctic sea ice cover. *Geophys. Res. Lett.* **2008**, *35*, L01703. https://doi.org/10.1029/2007GL031972.
66. Zhang, J.; Lindsay, R.; Schweiger, A.; Steele, M. The impact of an intense summer cyclone on 2012 Arctic sea ice retreat. *Geophys. Res. Lett.* **2013**, *40*, 720–726. https://doi.org/10.1002/GRL.50190.

67. Parkinson, C.L.; Comiso, J.C. On the 2012 record low Arctic sea ice cover: Combined impact of preconditioning and an August storm. *Geophys. Res. Lett.* **2013**, *40*, 1356–1361. https://doi.org/10.1002/GRL.50349.
68. Wang, Q.; Danilov, S.; Mu, L.; Sidorenko, D.; Wekerle, C. Lasting impact of winds on Arctic sea ice through the ocean's memory. *Cryosphere* **2021**, *15*, 4703–4725. https://doi.org/10.5194/tc-15-4703-2021.
69. Ukita, J.; Honda, M.; Nakamura, H.; Tachibana, Y.; Cavalieri, D.J.; Parkinson, C.L.; Koide, H.; Yamamoto, K. Northern Hemisphere sea ice variability: Lag structure and its implications. *Tellus A Dyn. Meteorol. Oceanogr.* **2016**, *59*, 261–272. https://doi.org/10.1111/j.1600-0870.2006.00223.x.
70. Deser, C.; Walsh, J.; Timlin, M. Arctic sea ice variability in the context of recent atmospheric circulation trends. trends. *J. Clim.* **2020**, *13*, 617–633.
71. Ding, Q.; Schweiger, A.; L'Heureux, M.; Battisti, D.S.; Po-Chedley, S.; Johnson, N.C.; Blanchard-Wrigglesworth, E.; Harnos, K.; Zhang, Q.; Eastman, R.; et al. Influence of high-latitude atmospheric circulation changes on summertime Arctic sea ice. *Nat. Clim. Chang.* **2017**, *7*, 289–295. https://doi.org/10.1038/nclimate3241.
72. Olonscheck, D.; Mauritsen, T.; Notz, D. Arctic sea-ice variability is primarily driven by atmospheric temperature fluctuations. *Nat. Geosci.* **2019**, *12*, 430–434. https://doi.org/10.1038/s41561-019-0363-1.
73. Flato, G.M.; Brown, R.D. Variability and climate sensitivity of landfast Arctic sea ice. *J. Geophys. Res. Ocean* **1996**, *101*, 25767–25777. https://doi.org/10.1029/96JC02431.
74. Howell, S.E.L.; Laliberté, F.; Kwok, R.; Derksen, C.; King, J. Landfast ice thickness in the Canadian Arctic Archipelago from observations and models. *Cryosphere* **2016**, *10*, 1463–1475. https://doi.org/10.5194/TC-10-1463-2016.
75. Ford, J.D.; McDowell, G.; Shirley, J.; Pitre, M.; Siewierski, R.; Gough, W.; Duerden, F.; Pearce, T.; Adams, P.; Statham, S. The Dynamic Multiscale Nature of Climate Change Vulnerability: An Inuit Harvesting Example. *Ann. Assoc. Am. Geogr.* **2013**, *103*, 1193–1211. https://doi.org/10.1080/00045608.2013.776880.
76. Arctic Monitoring and Assessment Programm. *Adaptation Actions for a Changing Arctic: Perspectives from the Bering-Chukchi-Beaufort Region*; AMAP: Oslo, Norway, 2017.
77. Ford, J.D.; Couture, N.; Bell, T.; Clark, D.G. Climate change and Canada's north coast: Research trends, progress, and future directions. *Environ. Rev.* **2017**, *26*, 82–92. https://doi.org/10.1139/ER-2017-0027.
78. Archer, L.; Ford, J.D.; Pearce, T.; Kowal, S.; Gough, W.A.; Allurut, M. Longitudinal assessment of climate vulnerability: A case study from the Canadian Arctic. *Sustain. Sci.* **2016**, *12*, 15–29. https://doi.org/10.1007/s11625-016-0401-5.
79. Lamontagne-Cumiford, M. The End of the Road: An Ethnographic Account of Tourism along the Inuvik-Tuktoyaktuk Highway. *Econ. Anthropol.* **2017**, *4*, 7–21. https://doi.org/10.1002/sea2.12069.
80. Divine, L.M.; Pearce, T.; Ford, J.; Solovyev, B.; Galappaththi, E.K.; Bluhm, B.; Kaiser, B.A. Protecting the future Arctic. *One Earth* **2021**, *4*, 1649–1651. https://doi.org/10.1016/j.oneear.2021.11.021.
81. Baztan, J.; Cordier, M.; Huctin, J.M.; Zhu, Z.; Vanderlinden, J.P. Life on thin ice: Insights from Uummannaq, Greenland for connecting climate science with Arctic communities. *Polar Sci.* **2017**, *13*, 100–108. https://doi.org/10.1016/J.POLAR.2017.05.002.
82. Karvonen, J. Estimation of Arctic land-fast ice cover based on dual-polarized Sentinel-1 SAR imagery. *Cryosphere* **2018**, *12*, 2595–2607. https://doi.org/10.5194/tc-12-2595-2018.